Supporting information

Hydronium-Ion-Catalyzed Elimination Pathways of Substituted Cyclohexanols in Zeolite H-ZSM5

Peter H. Hintermeier,[†] Sebastian Eckstein,[†] Donghai Mei,[‡] Mariefel V. Olarte,[‡] Donald M. Camaioni,[‡] Eszter Baráth,[†,*] and Johannes A. Lercher[†,‡,*]

[†]Technische Universität München, Department of Chemistry and Catalysis Research Center, Lichtenbergstraβe 4, Garching, D-85747, Germany

[‡]Institute for Integrated Catalysis, Pacific Northwest National Laboratory, 902 Battelle Boulevard, Richland, WA 99352, USA

Corresponding Authors

*E-mail: eszter.barath@tum.de, johannes.lercher@ch.tum.de

Table of contents

Experimental

Chemicals. The following chemicals were used: cyclohexanol (99%, *Sigma-Aldrich*), 4-methylcyclohexanol (mixture of *cis* and *trans* (25%:75%), 98%, *Sigma-Aldrich*), *cis*-4-methylcyclohexanol (> 98%, *Tokyo Chemical Industry*), *trans*-4-methylcyclohexanol (> 98%, *Tokyo Chemical Industry*), 3-methylcyclohexanol (mixture of *cis* and *trans* (43%:57%), > 98%, *Tokyo Chemical Industry*), 2-methylcyclohexanol (mixture of *cis* and *trans* (48%:52%), 99%, *Sigma-Aldrich*), *cis*-2-methylcyclohexanol (98%, *Sigma-Aldrich*), *trans*-2-methylcyclohexanol (99%, *Sigma-Aldrich*), 4-ethylcyclohexanol (mixture of *cis* and *trans* (31%:69%), > 97%, *Tokyo Chemical Industry*), 2-ethylcyclohexanol (mixture of *cis* and *trans* (75%:25%) > 97%, *Tokyo Chemical Industry*), 2-propylcyclohexanol (mixture of *cis* and *trans* (57%:43%), > 90%, *Tokyo Chemical Industry*), sodium sulfate (ACS reagent, > 99%, *Sigma-Aldrich*) ethyl acetate, (*Chromasolv*, 99.9%, *Sigma-Aldrich*), phosphoric acid (85% solution, *Sigma-Aldrich*) and sodium chloride (*ReagentPlus*, > 99%, *Sigma-Aldrich*). Hydrogen gas was obtained from *Westfalen* (> 99.999%). Deionized water was treated with an *Easypure-II* system from *WERNER* to obtain ultrapure water (18.2 MΩ·cm).

Zeolite catalyst. Zeolite MFI (Si/Al = 45) was obtained from *CLARIANT AG* in H-form and was treated at 550 °C (rate: 10 °C min^{-1}) for six hours in 100 mL min^{-1} synthetic air (80% nitrogen, 20% oxygen; >99%).

Catalyst stability experiments. 1.0 g of catalyst was stirred in the batch reactor at 190 °C and 50 bar for 14 hours. As an internal standard MgO was physically mixed with the parent and the treated zeolite in a 1:1 wt.% ratio. The MFI (22.5 and 25.0 2θ) and MgO reflexes (60.0 – 65.0 2θ) of the treated sample were integrated with GRAMS/AI (*Version 9.00R2 32*, Thermo Fisher Scientific) and compared to the parent MFI sample.

Reaction procedure and work-up method. All reactions were performed with the same molar amount of reactant, catalyst and solvent. In 100 mL ultrapure water 0.05 mol of substrate (5.01 g cyclohexanol, 5.71 g of 1-/2-/3-/4-methylcyclohexanol, 6.41 g of 2-/4-ethylcyclohexanol and 7.11 g of 2-propylcyclo-hexanol) and 50 mg of MFI zeolite were dissolved and suspended, respectively. The molar amount of reactant of pure *cis*- or *trans*-2-methylcyclohexanol was 4.38 mmol (0.5 g) in 100 mL water. In case of phosphoric acid, 5.0 mmol (342 µL or 0.58 g of 85% H_3PO_4), or 1.7 mmol (114 µL, 0.19 g of 85% H_3PO_4) were used in 100 mL water depending on reaction temperature.

The autoclave (300 mL) was loaded with 100 mL water, 50 mg MFI zeolite catalyst and 0.05 mol of (substituted) cyclohexanol substrate. The reactor was purged two times (20 bar) with hydrogen and was heated to the desired temperature at a pressure of 20 bar hydrogen at the start without stirring. Ten degrees

below the reaction temperature the total pressure of the reactor was adjusted to 50 bar with hydrogen gas and as soon as the reaction temperature was reached the stirring rate was set to 700 rpm. After the reaction time, the reactor was cooled using an ice bath. The pressure within the reactor was released below a temperature of 5 °C to prevent the loss of volatile products (cyclohexene). The reaction mixture was extracted with 3 x 20 mL ethyl acetate. To improve the phase separation of the organic and the aqueous phases, a small amount of sodium chloride was added to the reaction mixture. After extraction, the organic phase was dried over sodium sulfate and analyzed by GC-MS. The carbon-balance was monitored (95-99%) by an internal standard (dodecane).

Reactor. All reactions were performed in an autoclave (300 mL) from *Parr Instruments Co.* (type: *PST FS*, material: HASTELLOY C) with a temperature and stirring controlling device (*Parr Instruments Co. 4848 Reactor Controller*).

GC-MS. Quantification and qualification of the dehydration reactions was analyzed by GC/MS (*Agilent Technologies 7890 B GC*, column: *Agilent 19091S-433UI INV02* (30 m x 250 µm x 0.25 µm), heating program: 10 °C min^{-1} from 80 °C to 280 °C). Data was analyzed with *MassHunter Workstation Software, Qualitative Analysis, Version B.06.00, Agilent Technologies (2012).* An aliquot of the worked-up reaction mixture (1 µl) was injected to the GC-MS.

AAS. The Si and Al content of the MFI zeolite sample was determined by atomic absorption spectroscopy (AAS) on a *UNICAM 939 AA–Spectrometer*.

N_2 physisorption. The specific surface area and pore volume of the zeolite were determined by nitrogen physisorption. The isotherms were measured at liquid nitrogen temperature (-196 °C) using a *PMI Automatic Sorptometer*. The catalyst was activated in vacuum at 200 °C for two hours before measurement. Apparent surface area was calculated by applying the *Brunauer-Emmett-Teller (BET)* theory, and the *t-plot method* was used to determine the pore volumes.

SEM. The scanning electron microscopy (SEM) images were recorded on a *JEOL 500 SEM-microscopy* (accelerating voltage: 25 kV). The samples were prepared by depositing a drop of an ultrasonicated methanol suspension of the solid material onto a carbon-coated Cu grid.

XRD. The crystal structures of the zeolites were analyzed by X-ray powder diffraction (XRD) using a *Philips X'Pert Pro system*, with Cu-K_α radiation operating at 45 kV/40 mA. The sample was measured with a scanning rate of 0.017°/s in the range from 5 to 70° (2θ).

IR. Infrared spectroscopy of adsorbed pyridine was performed with a *Perkin–Elmer 2000* spectrometer at a resolution of 4 cm^{-1}. The catalyst sample was prepared as wafer and activated in vacuum (ca. 10^{-6} mbar)

at 450 °C for one hour (heating rate = 10 °C min^{-1}). After this, at 150 °C the sample was equilibrated with 0.1 mbar of pyridine for 30 min followed by outgassing for one hour. A spectrum with the chemisorbed pyridine was recorded thereafter. Adsorbed pyridine was desorbed finally by heating up to 450 °C at 10 °C min^{-1} for half an hour. Again the spectra were recorded at equilibrium. For quantification, molar integral extinction coefficients of 0.73 cm μmol^{-1} and 0.96 cm μmol^{-1} were used for Brønsted and Lewis acid sites respectively.

^{1}H NMR. ^{1}H NMR spectra with water signal suppression were recorded at 30 °C using an *Avance III HD 500 System* (Bruker Biospin, Rheinstetten, Germany) with an Ultra-Shield 500 MHz magnet (11.75 T) and a BBI 500 S2 probe head (5 mm, inverse 1H/X with Z-gradient). Quantification of *cis/trans* isomers before reaction was obtained by the integrated signal intensities in $CDCl_3$ (reference). Quantification of *cis/trans* isomers after reaction (aqueous phase) was obtained by measurements in D_2O on the basis of the integrated signal intensities. Characteristic signals at chemical shifts were: *cis*-2-McyOH (~3.8 ppm), *trans*-2-McyOH (~3.1 – 3.2 ppm), *cis*-4-McyOH (~3.9 – 4.0 ppm) and *trans*-4-McyOH (~3.5 – 3.6 ppm).

NH_3-TPD. Temperature-programmed desorption (TPD) of ammonia was performed in a 6-fold parallel reactor system. The catalysts were activated under reduced pressure at 450 °C (heating rate: 5 °C min^{-1}) for one hour. NH_3 was adsorbed for one hour with a partial pressure of 1 mbar at 100 °C, respectively. Subsequently, the samples were evacuated for two hours in order to remove physisorbed probe molecules. For the temperature-programmed desorption experiments, six samples were sequentially heated from 100 to 770 °C with a heating rate of 10 °C min^{-1} to desorb ammonia. The rates of desorbing species were monitored by mass spectrometry (*Balzers QME 200*). For the quantification of the amount of acidity, a standard MFI zeolite with known acid site concentration was used to calibrate the signal.

Calculations. The activation parameters for the dehydration of an alcohol are based on calculations considering the conversion. The activation parameters for a special product (e.g. Saytzeff- or Hofmann-product) are based on calculations considering the yield of the product. **Conversion** = (mole of converted reactant / mole of the starting reactant) × 100%. **Yield** = (mole of formed product / mole of starting reactant) × (stoichiometric coefficient of reactant / stoichiometric coefficient of proudct) × 100%. **Selectivity** = mole of product / (mole of converted reactant) × 100%. **The (initial) reaction rate** was deduced from the slope of the linear fit to the conversion versus time plot in the linear region at low conversions (≤ 20%). **TOF** = mole of converted reactant / (mole of accessible acid sites × reaction time). **The carbon balance** = (mole of carbon in the product / mole of carbon in starting reactant) × 100%.

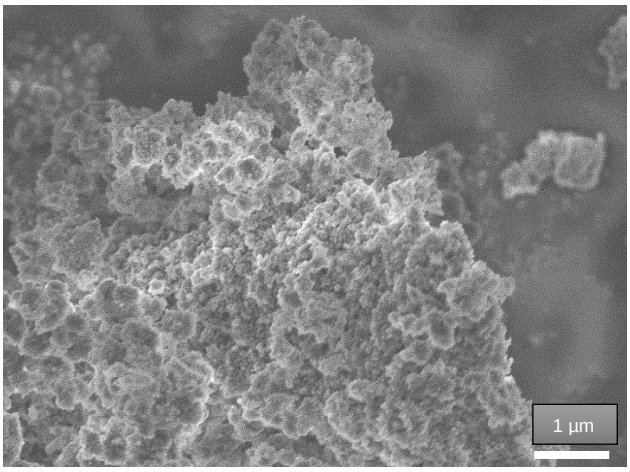

Figure S1. MFI-45 (Si/Al = 45).

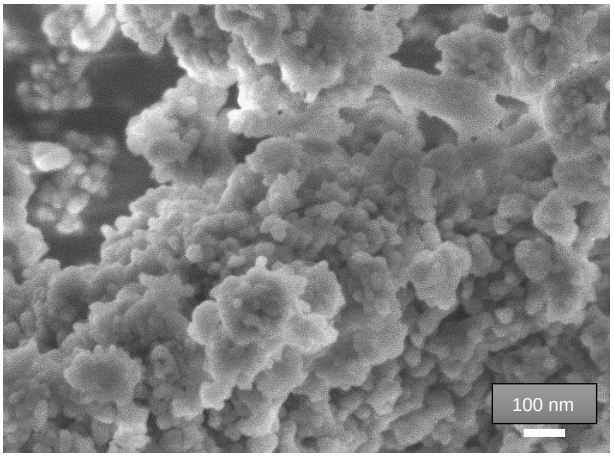

Figure S2. MFI-45 (Si/Al = 45).

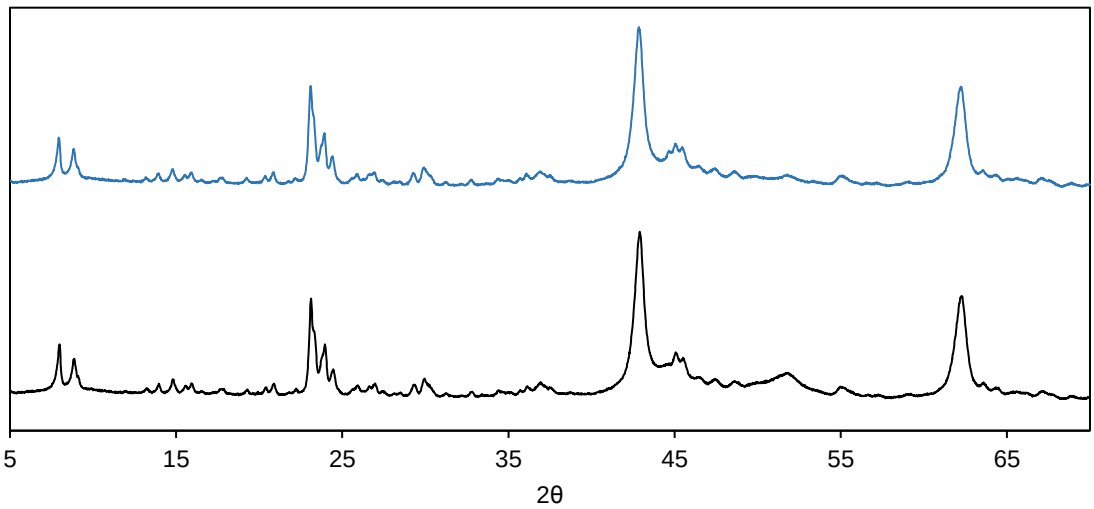

Figure S3. X-Ray diffraction pattern of the treated (blue; 190 °C, 14h) and parent (black) **MFI-45** (internal standard MgO).

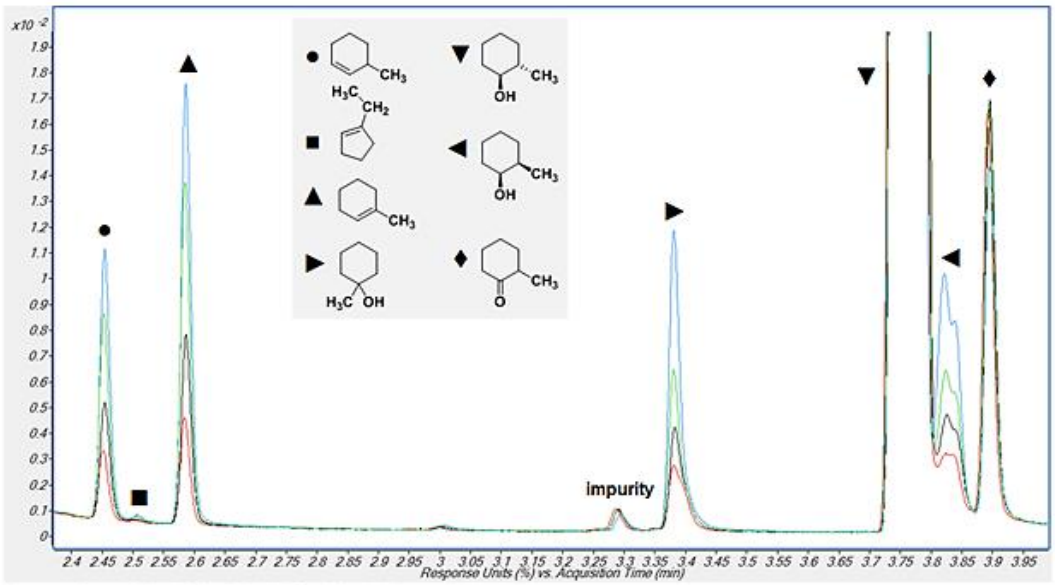

Figure S4. Dehydration of *trans*-2-McyOH forms *cis*-2-McyOH *via* rehydration (initial impurity of *cis*-2-McyOH: ca. 1%). ● Hofmann-product; ■ 1-ethylcyclopent-1-ene; ▲ Saytzeff-product; ► 1-McyOH; ▼ *trans*-2-McyOH; ◄ *cis*-2-McyOH; ♦ 2-methyl-cyclohexan-1-one (impurity).

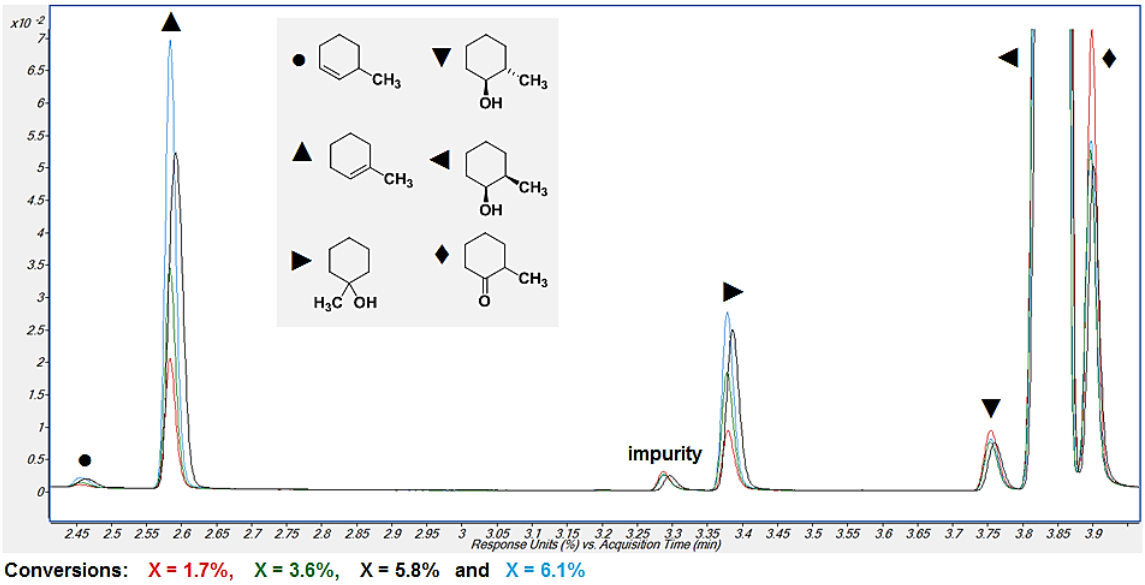

Figure S5. Dehydration of *cis*-2-McyOH does not form *trans*-2-McyOH (initial impurity of *trans*-2-McyOH: ca. 1%). ● Hofmann-product; ▲ Saytzeff-product; ► 1-McyOH; ▼ *trans*-2-McyOH (impurity); ◄ *cis*-2-McyOH; ♦ 2-methyl-cyclohexan-1-one (impurity).

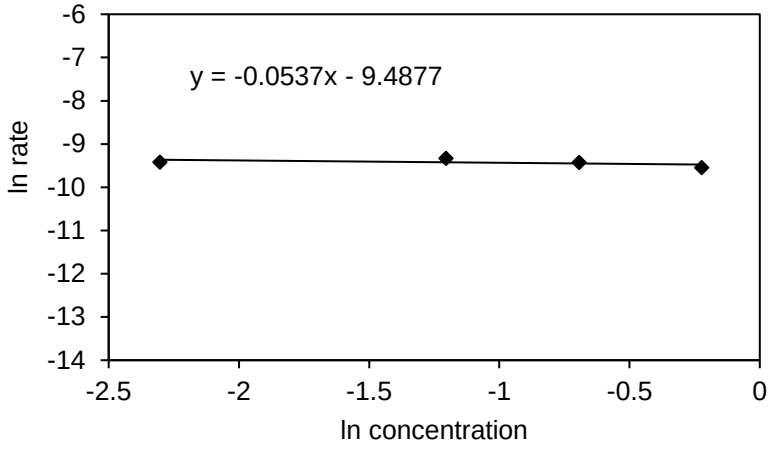

Figure S6. Reaction order of **CyOH** dehydration (170 °C, 50 bar, **MFI-45**).

Table S1. Dehydration rates and initial concentrations of **CyOH** dehydration (170 °C, 50 bar, **MFI-45**).

rate (mol g^{-1} s^{-1})	n (mol)	c (mol L^{-1})	ln rate	ln c
7.2×10^{-5}	0.08	0.80	-9.54	-0.22
8.1×10^{-5}	0.05	0.50	- 9.43	-0.69
8.9×10^{-5}	0.03	0.30	- 9.33	-1.20
8.2×10^{-5}	0.01	0.10	-9.41	-2.30

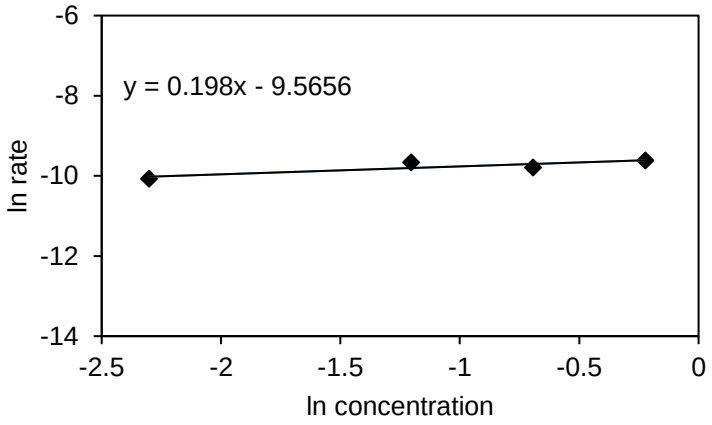

Figure S7. Reaction order of **2-McyOH** dehydration (170 °C, 50 bar, **MFI-45**).

Table S2. Dehydration rates and initial concentration of **2-McyOH** (170 °C, 50 bar, **MFI-45**).

rate (mol g^{-1} s^{-1})	n (mol)	c (mol L^{-1})	ln rate	ln c
6.7×10^{-5}	0.08	0.80	- 9.62	-0.22
5.6×10^{-5}	0.05	0.50	- 9.79	-0.69
6.4×10^{-5}	0.03	0.30	- 9.66	-1.20
4.2×10^{-5}	0.01	0.10	-10.07	-2.30

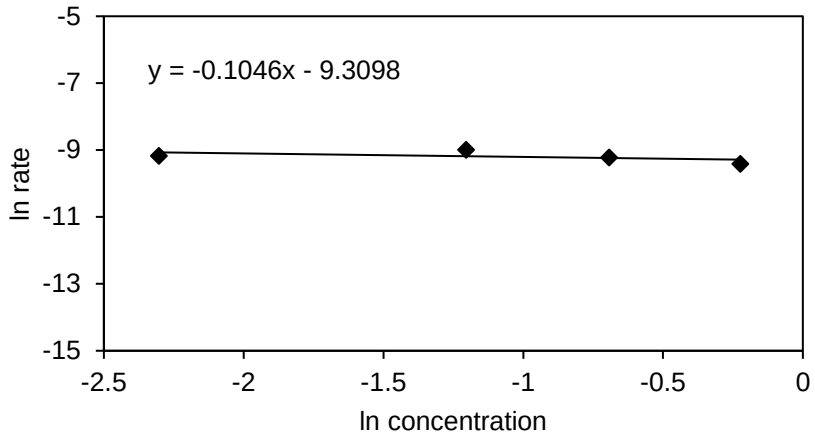

Figure S8. Reaction order of **4-McyOH** dehydration (180 °C, 50 bar, **MFI-45**).

Table S3. Dehydration rates and initial concentration **of 4-McyOH** (180 °C, 50 bar, **MFI-45**).

rate (mol g^{-1} s^{-1})	n (mol)	c (mol L^{-1})	ln rate	ln c
8.2×10^{-5}	0.08	0.80	- 9.41	-0.22
9.9×10^{-5}	0.05	0.50	- 9.22	-0.69
1.3×10^{-4}	0.03	0.30	- 8.98	-1.20
1.0×10^{-4}	0.01	0.10	- 9.20	-2.30

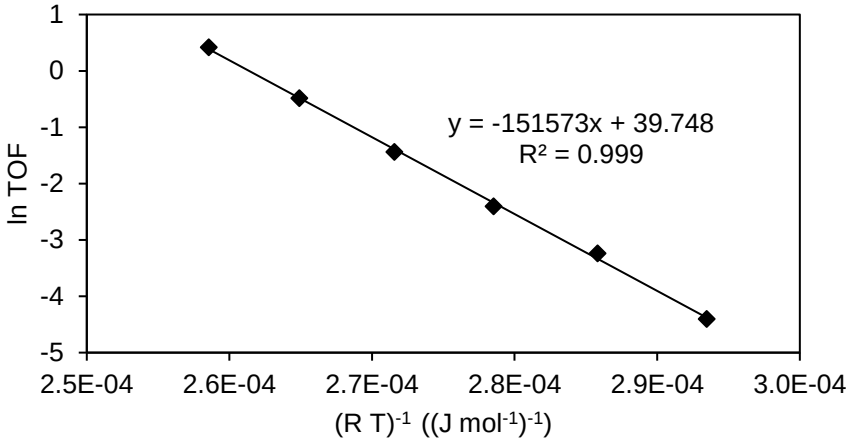

Figure S9. Arrhenius-plot: **CyOH** (0.5 M) dehydration ($E_a \approx 152$ kJ mol^{-1}), **MFI-45**.

Table S4. CyOH (0.5 M) dehydration rates at different reaction temperatures, **MFI-45**.

T (°C)	T (K)	TOF (s^{-1})	rate (mol g^{-1} s^{-1})	$(R\ T)^{-1}$ [$(J\ mol^{-1})^{-1}$]	ln TOF
140	413	1.2×10^{-2}	4.4×10^{-6}	2.91×10^{-4}	-4.4
150	423	3.9×10^{-2}	1.4×10^{-5}	2.84×10^{-4}	-3.2
160	433	9.1×10^{-2}	3.3×10^{-5}	2.78×10^{-4}	-2.4
170	443	2.4×10^{-1}	8.6×10^{-5}	2.71×10^{-4}	-1.4
180	453	6.2×10^{-1}	2.2×10^{-4}	2.65×10^{-4}	-0.5
190	463	1.5	5.5×10^{-4}	2.60×10^{-4}	+0.4

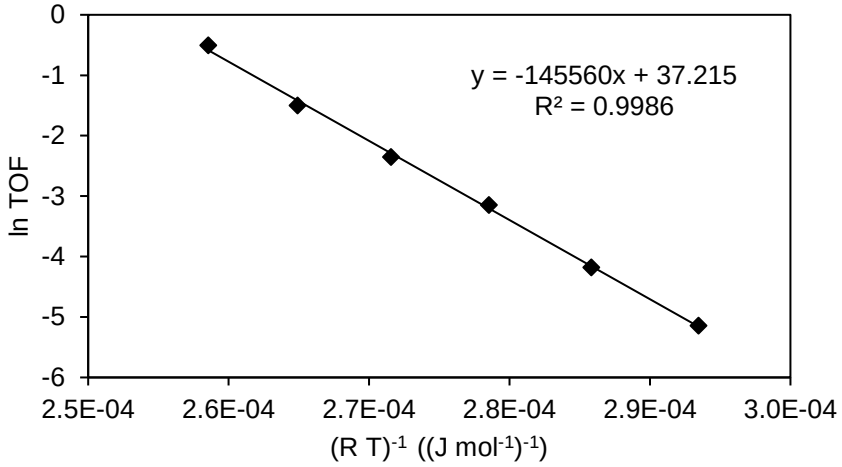

Figure S10. Arrhenius-plot: **4-McyOH** (0.5 M) dehydration ($E_a \approx 146$ kJ mol^{-1}), **MFI-45**.

Table S5. 4-McyOH (0.5 M) dehydration rates at different reaction temperatures, **MFI-45**.

T (°C)	T (K)	TOF (s^{-1})	rate (mol g^{-1} s^{-1})	$(R\ T)^{-1}$ [$(J\ mol^{-1})^{-1}$]	ln TOF
140	413	5.8×10^{-3}	2.1×10^{-6}	2.91×10^{-4}	-5.1
150	423	1.5×10^{-2}	5.5×10^{-6}	2.84×10^{-4}	-4.2
160	433	4.3×10^{-2}	1.6×10^{-5}	2.78×10^{-4}	-3.1
170	443	9.5×10^{-2}	3.4×10^{-5}	2.71×10^{-4}	-2.4
180	453	2.2×10^{-1}	8.1×10^{-5}	2.65×10^{-4}	-1.5
190	463	6.0×10^{-1}	2.2×10^{-4}	2.60×10^{-4}	-0.5

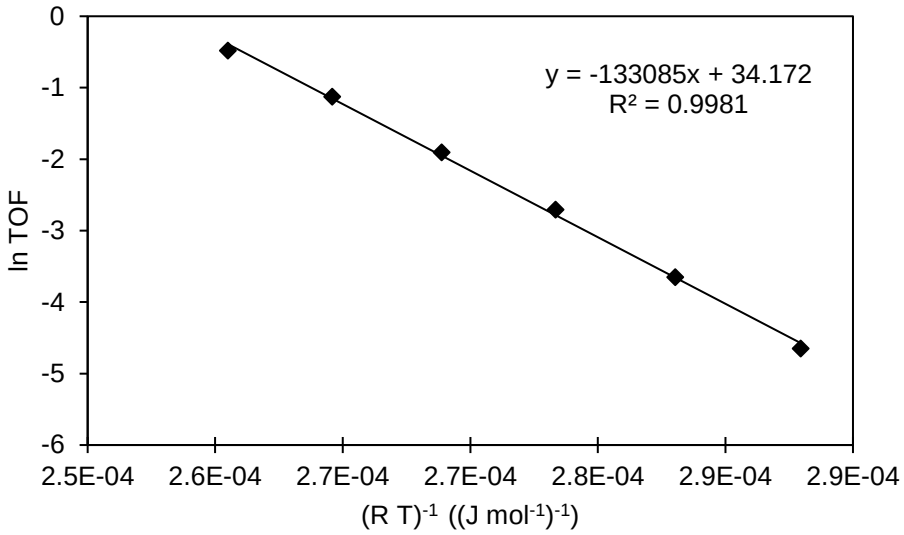

Figure S11. Arrhenius-plot: **3-McyOH** (0.5 M) dehydration ($E_a \approx 133$ kJ mol^{-1}), **MFI-45**.

Table S6. 3-McyOH (0.5 M) dehydration rates at different reaction temperatures, **MFI-45**.

T (°C)	T (K)	TOF (s^{-1})	rate (mol g^{-1} s^{-1})	$(R\ T)^{-1}$ [$(J\ mol^{-1})^{-1}$]	ln TOF
140	413	9.6×10^{-3}	3.5×10^{-6}	2.91×10^{-4}	-4.6
150	423	2.6×10^{-2}	9.4×10^{-6}	2.84×10^{-4}	-3.6
160	433	6.7×10^{-2}	2.4×10^{-5}	2.78×10^{-4}	-2.7
170	443	1.5×10^{-1}	5.4×10^{-5}	2.71×10^{-4}	-1.9
180	453	3.3×10^{-1}	1.2×10^{-4}	2.65×10^{-4}	-1.1
190	463	6.2×10^{-1}	2.2×10^{-4}	2.60×10^{-4}	-0.5

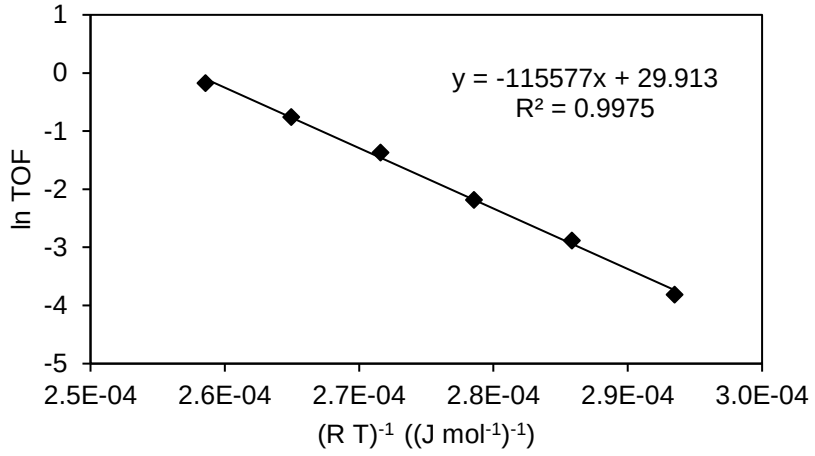

Figure S12. Arrhenius-plot: **2-McyOH** (0.5 M) dehydration ($E_a \approx 116$ kJ mol^{-1}), **MFI-45**.

Table S7. 2-McyOH (0.5 M) dehydration rates at different reaction temperatures, **MFI-45**.

T (°C)	T (K)	TOF (s^{-1})	rate (mol g^{-1} s^{-1})	$(R\ T)^{-1}$ [(J $mol^{-1})^{-1}$]	ln TOF
140	413	2.2×10^{-2}	7.9×10^{-6}	2.91×10^{-4}	-3.8
150	423	5.6×10^{-2}	2.0×10^{-5}	2.84×10^{-4}	-2.9
160	433	1.1×10^{-1}	4.0×10^{-5}	2.78×10^{-4}	-2.2
170	443	2.5×10^{-1}	9.2×10^{-5}	2.71×10^{-4}	-1.4
180	453	4.7×10^{-1}	1.7×10^{-4}	2.65×10^{-4}	-0.8
190	463	8.4×10^{-1}	3.0×10^{-4}	2.60×10^{-4}	-0.2

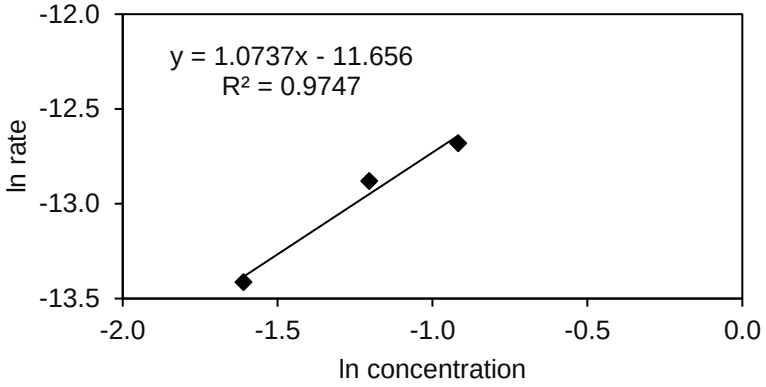

Figure S13. Reaction order of **2-McyOH** dehydration (170 °C, 50 bar, **H_3PO_4**).

Table S8. Dehydration rates and initial concentrations of **2-McyOH (**170 °C, 50bar, **H_3PO_4)**.

c (mol L^{-1})	rate (mol s^{-1})	ln c	ln rate
0.2	1.5×10^{-6}	-1.61	-13.41
0.3	2.6×10^{-6}	-1.20	-12.88
0.4	3.1×10^{-6}	-0.92	-12.68

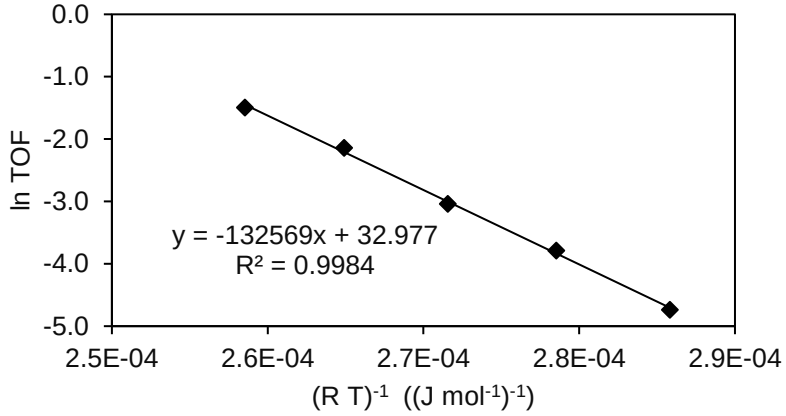

Figure S14. Arrhenius-plot: **2-McyOH** (0.2 M) dehydration ($E_a \approx 133$ kJ mol^{-1}), **H_3PO_4**.

Table S9. 2-McyOH (0.2 M) dehydration rates at different reaction temperatures, **H_3PO_4**.

T (°C)	T (K)	rate (mol s^{-1})	k (L mol^{-1} s^{-1})	n H^+ (mmol)	ln k	$(R\ T)^{-1}$ $[(J\ mol^{-1})^{-1}]$
150	423	3.2×10^{-7}	8.8×10^{-3}	1.83×10^{-1}	-4.74	2.84×10^{-4}
160	433	7.5×10^{-7}	2.3×10^{-2}	1.66×10^{-1}	-3.79	2.78×10^{-4}
170	443	1.4×10^{-6}	4.8×10^{-2}	1.51×10^{-1}	-3.04	2.71×10^{-4}
180	453	3.2×10^{-6}	1.2×10^{-1}	1.36×10^{-1}	-2.14	2.65×10^{-4}
190	463	5.5×10^{-6}	2.2×10^{-1}	1.23×10^{-1}	-1.50	2.60×10^{-4}

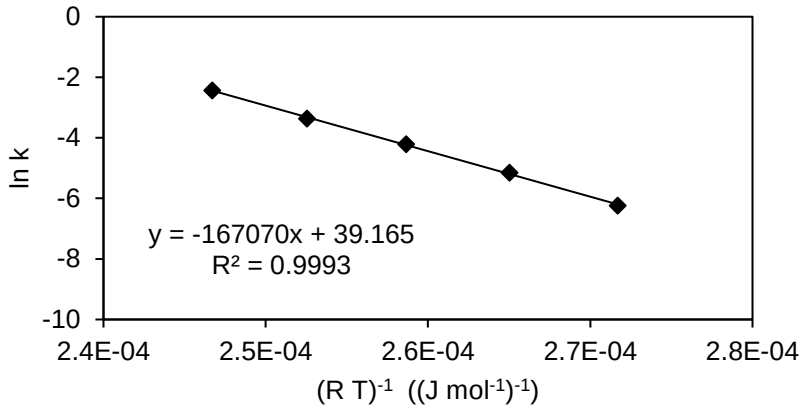

Figure S15. Arrhenius-plot: ***trans*-2-McyOH** (0.04 M) dehydration ($E_a \approx 167$ kJ mol^{-1}), **H_3PO_4**.

Table S10. *trans*-2-McyOH (0.04 M) dehydration rates at different reaction temperatures, **H_3PO_4**.

T (°C)	T (K)	rate (mol s^{-1})	n H^+ (mol)	k (L mol^{-1} s^{-1})	ln k	$(R\ T)^{-1}$ $[(J\ mol^{-1})^{-1}]$
170	443	5.3×10^{-8}	6.2×10^{-4}	2.0×10^{-3}	-6.24	2.72×10^{-4}
180	453	1.4×10^{-7}	5.6×10^{-4}	5.8×10^{-3}	-5.15	2.66×10^{-4}
190	463	3.3×10^{-7}	5.1×10^{-4}	1.5×10^{-2}	-4.21	2.60×10^{-4}
200	473	4.1×10^{-7}	2.7×10^{-4}	3.5×10^{-2}	-3.36	2.54×10^{-4}
210	483	9.2×10^{-7}	2.4×10^{-4}	8.7×10^{-2}	-2.44	2.49×10^{-4}

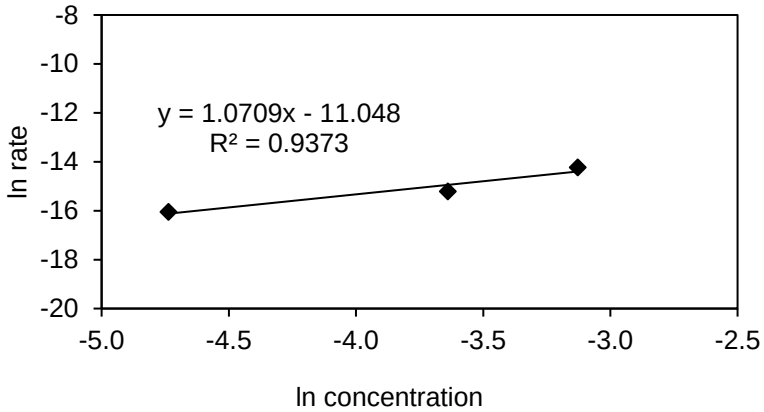

Figure S16. Reaction order for ***trans*-2-McyOH** dehydration (190 °C, 50 bar, **H_3PO_4**).

Table S11. ***Trans*-2-McyOH** dehydration rates for different initial concentrations (190 °C, 50 bar, **H_3PO_4**).

c (mmol L^{-1})	rate (mol s^{-1})	ln rate	ln c
8.8	1.58×10^{-7}	- 16.0	- 4.7
26.3	2.26×10^{-7}	- 15.2	- 3.6
43.8	6.66×10^{-7}	- 14.2	- 3.1

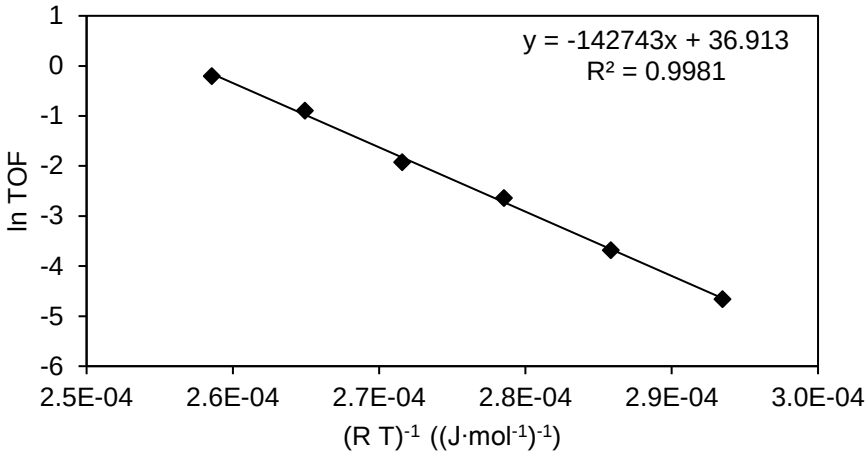

Figure S17. Arrhenius-plot: **4-EcyOH** (0.5 M) dehydration ($E_a \approx 143$ kJ mol^{-1}), **MFI-45**.

Table S12. 4-EcyOH (0.5 M) dehydration rates at different reaction temperatures, **MFI-45**.

T (°C)	T (K)	TOF (s^{-1})	rate (mol s^{-1})	$(R\,T)^{-1}$ [(J mol^{-1})$^{-1}$]	ln TOF
140	413	9.5×10^{-3}	3.4×10^{-6}	2.91×10^{-4}	-4.7
150	423	2.5×10^{-2}	9.1×10^{-6}	2.84×10^{-4}	-3.7
160	433	7.2×10^{-2}	2.6×10^{-5}	2.78×10^{-4}	-2.6
170	443	1.5×10^{-1}	5.3×10^{-5}	2.71×10^{-4}	-1.9
180	453	4.1×10^{-1}	1.5×10^{-4}	2.65×10^{-4}	-0.9
190	463	8.2×10^{-1}	2.9×10^{-4}	2.60×10^{-4}	-0.2

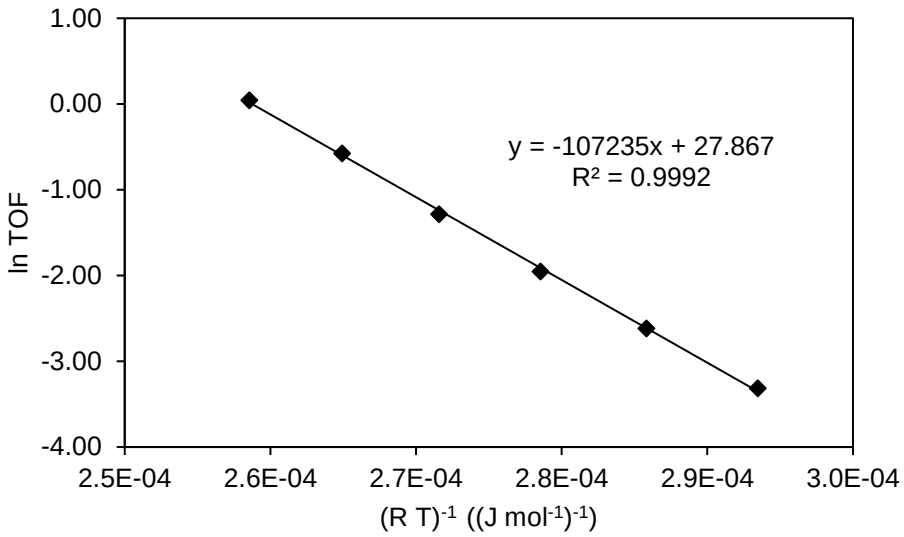

Figure S18. Arrhenius-plot: **2-EcyOH** (0.5 M) dehydration ($E_a \approx 107$ kJ mol^{-1}), **MFI-45**.

Table S13. 2-EcyOH (0.5 M) dehydration rates at different reaction temperatures, **MFI-45**.

T (°C)	T (K)	TOF (s^{-1})	rate (mol g^{-1} s^{-1})	$(R\ T)^{-1}$ [$(J\ mol^{-1})^{-1}$]	ln TOF
140	413	3.6×10^{-2}	1.3×10^{-5}	2.91×10^{-4}	-3.3
150	423	7.3×10^{-2}	2.6×10^{-5}	2.84×10^{-4}	-2.6
160	433	1.4×10^{-1}	5.1×10^{-5}	2.78×10^{-4}	-2.0
170	443	2.8×10^{-1}	1.0×10^{-4}	2.71×10^{-4}	-1.3
180	453	5.6×10^{-1}	2.0×10^{-4}	2.65×10^{-4}	-0.6
190	463	1.0	3.8×10^{-4}	2.60×10^{-4}	-0.0

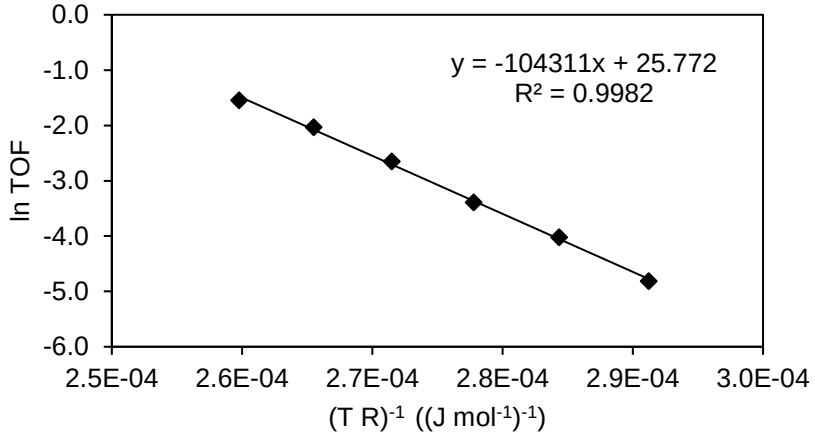

Figure S19. Arrhenius-plot: **2-PcyOH** (0.5 M) dehydration ($E_a \approx 104$ kJ mol^{-1}), **MFI-45**.

Table S14. 2-PcyOH (0.5 M) dehydration rates at different reaction temperatures, **MFI-45**.

T (°C)	T (K)	TOF (s^{-1})	rate (mol g^{-1} s^{-1})	$(R\ T)^{-1}$ [$(J\ mol^{-1})^{-1}$]	ln TOF
140	413	8.1×10^{-3}	2.9×10^{-6}	2.91×10^{-4}	-4.8
150	423	1.8×10^{-2}	6.5×10^{-6}	2.84×10^{-4}	-4.0
160	433	3.4×10^{-2}	1.4×10^{-5}	2.78×10^{-4}	-3.4
170	443	7.1×10^{-2}	2.5×10^{-5}	2.71×10^{-4}	-2.7
180	453	1.3×10^{-1}	4.7×10^{-5}	2.65×10^{-4}	-2.0
190	463	2.1×10^{-1}	7.7×10^{-5}	2.60×10^{-4}	-1.5

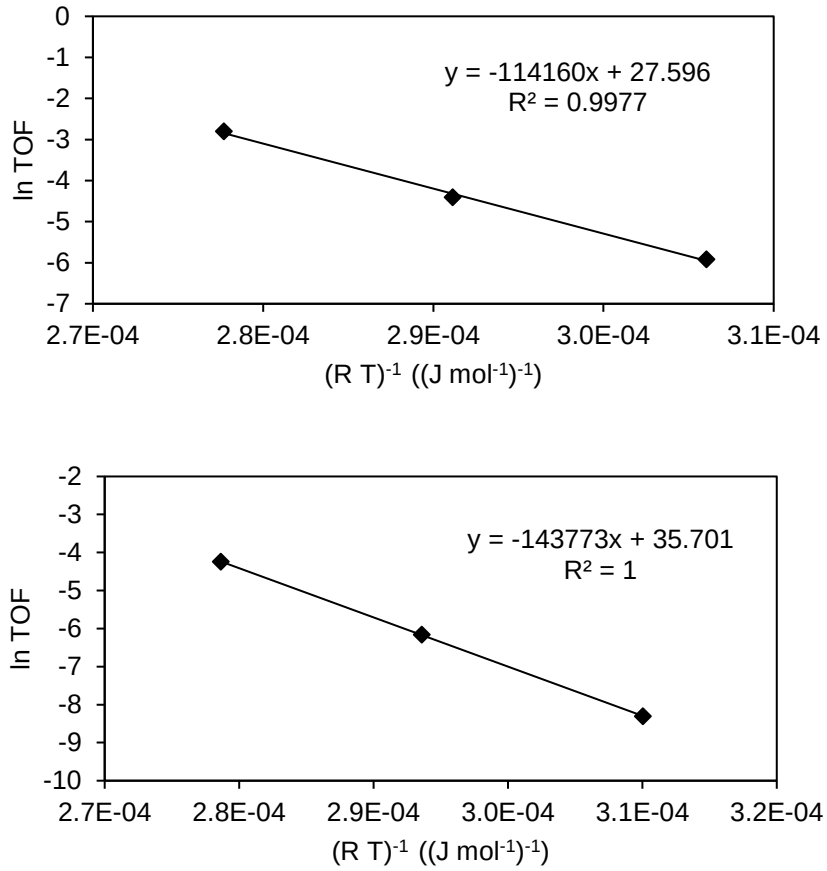

Figure S20. Arrhenius-plot: pure isomers of 2-methylcyclohexanol (0.04 M), ***cis*-2-McyOH** (top; E_a = 114 kJ mol^{-1}) and ***trans*-2-McyOH** (bottom; $E_a \approx$ 144 kJ mol^{-1}), **MFI-45**.

Table S15. ***Cis*-2-McyOH** (0.04 M, top) and ***trans*-2-McyOH** (0.04 M, bottom) dehydration rates, **MFI-45**.

T (°C)	T (K)	TOF (s^{-1})	rate (mol g^{-1} s^{-1})	$(R\ T)^{-1}$ [$(J\ mol^{-1})^{-1}$]	ln TOF
120	393	2.7×10^{-3}	9.7×10^{-7}	3.06×10^{-4}	-5.9
140	413	1.2×10^{-2}	4.4×10^{-6}	2.91×10^{-4}	-4.4
160	433	6.1×10^{-2}	2.5×10^{-5}	2.78×10^{-4}	-2.8

T (°C)	T (K)	TOF (s^{-1})	rate (mol g^{-1} s^{-1})	$(R\ T)^{-1}$ [$(J\ mol^{-1})^{-1}$]	ln TOF
120	393	2.5×10^{-4}	8.9×10^{-8}	3.06×10^{-4}	-8.3
140	413	2.1×10^{-3}	7.6×10^{-7}	2.91×10^{-4}	-6.2
160	433	1.4×10^{-2}	5.2×10^{-6}	2.78×10^{-4}	-4.2

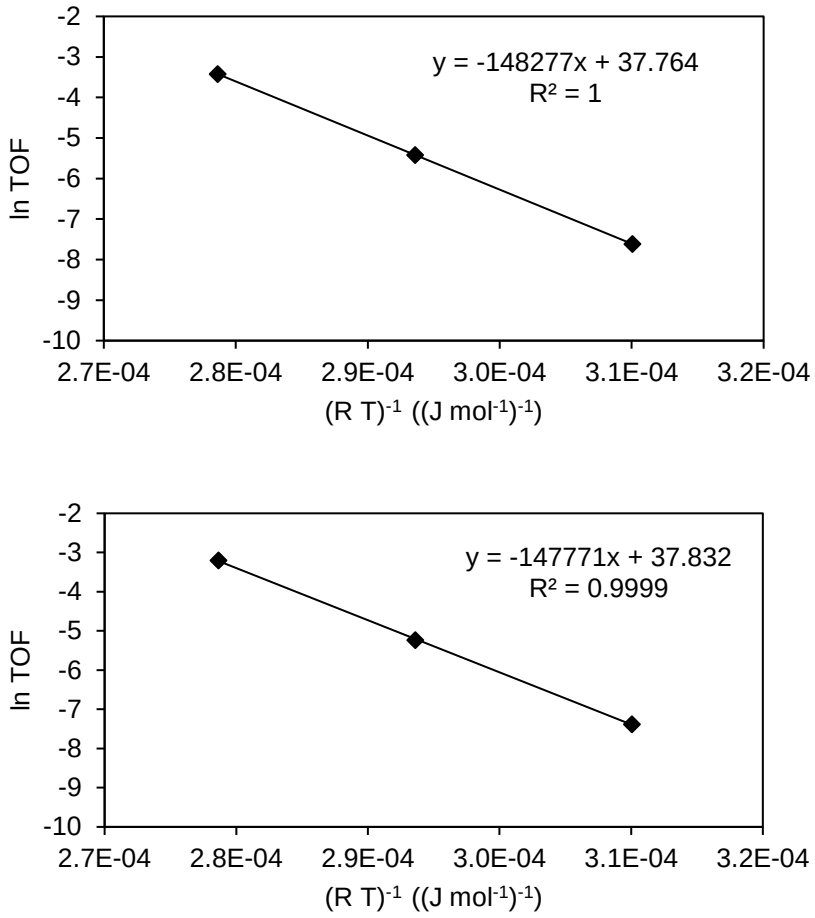

Figure 21. Arrhenius-plot: pure isomers of 4-methylcyclohexanol (0.04 M), ***cis*-4-McyOH** (top; E_a = 148 kJ mol^{-1}) and ***trans*-4-McyOH** (bottom; $E_a \approx$ 148 kJ mol^{-1}), **MFI-45**.

Table S16. ***Cis*-4-McyOH** (0.04 M, top) and ***trans*-4-McyOH** dehydration rates (0.04 M, bottom) at different reaction temperatures, **MFI-45**.

T (°C)	T (K)	TOF (s^{-1})	rate (mol g^{-1} s^{-1})	$(R\ T)^{-1}$ [$(J\ mol^{-1})^{-1}$]	ln TOF
120	393	4.9×10^{-4}	1.8×10^{-7}	3.06×10^{-4}	-7.6
140	413	4.4×10^{-3}	1.6×10^{-6}	2.91×10^{-4}	-5.4
160	433	3.3×10^{-2}	1.2×10^{-5}	2.78×10^{-4}	-3.4

T (°C)	T (K)	TOF (s^{-1})	rate (mol g^{-1} s^{-1})	$(R\ T)^{-1}$ [$(J\ mol^{-1})^{-1}$]	ln TOF
120	393	6.2×10^{-4}	2.2×10^{-7}	3.06×10^{-4}	-7.4
140	413	5.4×10^{-3}	1.9×10^{-6}	2.91×10^{-4}	-5.2
160	433	4.1×10^{-2}	1.5×10^{-5}	2.78×10^{-4}	-3.2

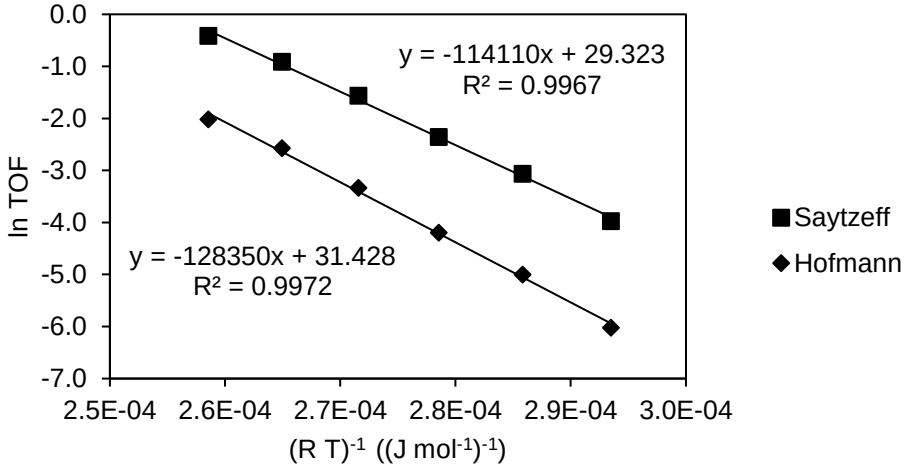

Figure S22. Arrhenius-plot: Hofmann- and Saytzeff-product (E_a = 114 and 128 kJ mol^{-1}) of **2-McyOH** (0.5 M), **MFI-45**.

Table S17. Dehydration rates leading to Hofmann- and Saytzeff-products of **2-McyOH** (0.5 M), **MFI-45**.

T (°C)	T (K)	rate Hofmann-product (mol s^{-1} g^{-1})	rate Saytzeff-product (mol s^{-1} g^{-1})	$(R\ T)^{-1}$ ($(J\ mol^{-1})^{-1}$)	ln TOF Saytzeff-product	ln TOF Hofmann-product
140	413	8.7×10^{-7}	6.7×10^{-6}	2.91×10^{-4}	-6.0	-4.0
150	423	2.4×10^{-6}	1.7×10^{-5}	2.84×10^{-4}	-5.0	-3.1
160	433	5.4×10^{-6}	3.4×10^{-5}	2.78×10^{-4}	-4.2	-2.4
170	443	1.3×10^{-5}	7.5×10^{-5}	2.71×10^{-4}	-3.3	-1.6
180	453	2.7×10^{-5}	1.4×10^{-4}	2.65×10^{-4}	-2.6	-0.9
190	463	4.8×10^{-5}	2.4×10^{-4}	2.60×10^{-4}	-2.0	-0.4

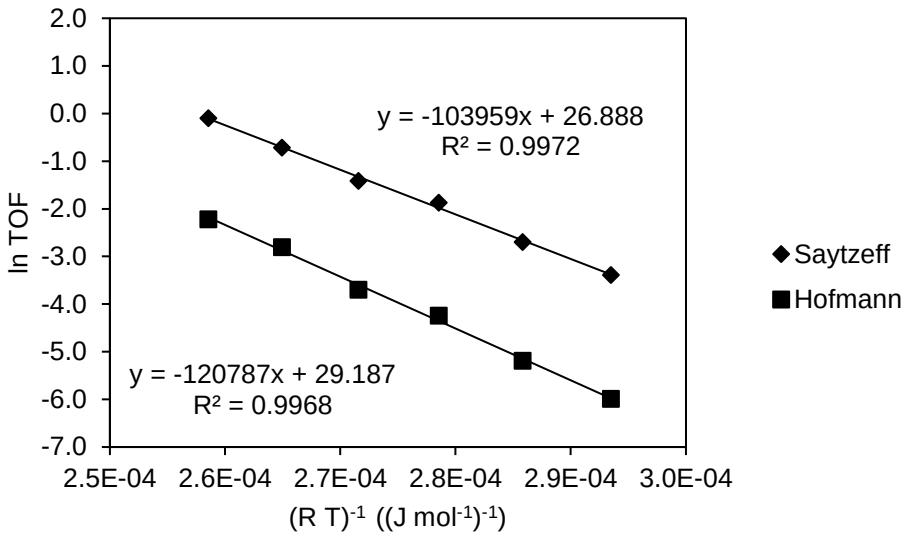

Figure S23. Arrhenius-*plot*: Hofmann- and Saytzeff-product (E_a = 104 and 121 kJ mol^{-1}) of **2-EcyOH** (0.5 M), **MFI-45**.

Table S18. Dehydration rates leading to Hofmann- and Saytzeff-products of **2-EcyOH** (0.5 M), **MFI-45**.

T (°C)	T (K)	rate Hofmann-product (mol s^{-1} g^{-1})	rate Saytzeff-product (mol s^{-1} g^{-1})	(R T)$^{-1}$ ((J mol^{-1})$^{-1}$)	ln TOF Saytzeff-product	ln TOF Hofmann-product
140	413	9.1×10^{-7}	1.2×10^{-5}	2.91×10^{-4}	-3.4	-6.0
150	423	2.0×10^{-6}	2.4×10^{-5}	2.84×10^{-4}	-2.7	-5.2
160	433	5.2×10^{-6}	5.6×10^{-5}	2.78×10^{-4}	-1.9	-4.2
170	443	8.9×10^{-6}	8.8×10^{-5}	2.71×10^{-4}	-1.4	-3.7
180	453	2.2×10^{-5}	1.8×10^{-4}	2.65×10^{-4}	-0.7	-2.8
190	463	3.9×10^{-5}	3.3×10^{-4}	2.60×10^{-4}	-0.1	-2.2

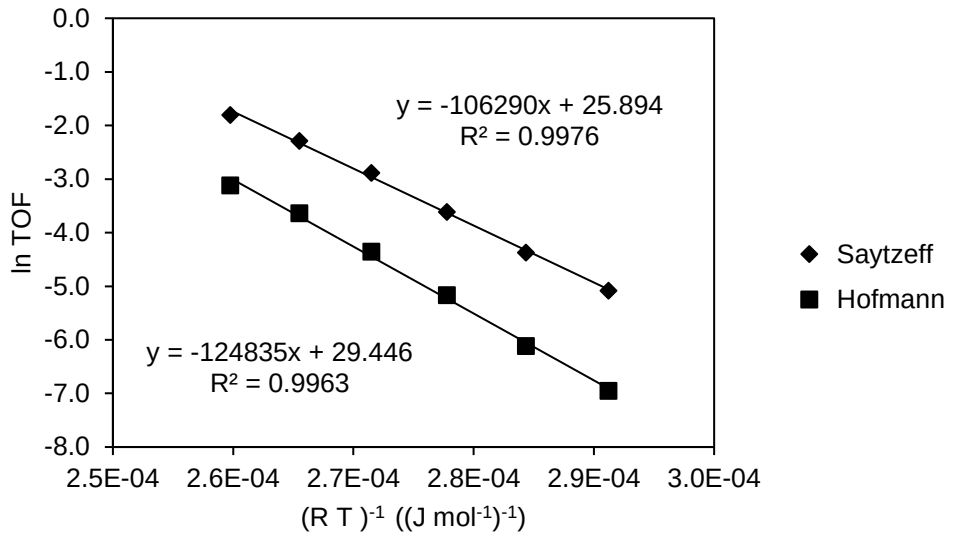

Figure S24. Arrhenius-plot: Hofmann- and Saytzeff-product (E_a = 106 and 125 kJ mol^{-1}) s of **2-PcyOH** (0.5 M), **MFI-45**.

Table S19. Dehydration rates leading to Hofmann- and Saytzeff-products of **2-PcyOH** (0.5 M), **MFI-45**.

T (°C)	T (K)	rate Saytzeff-product (mol s^{-1} g^{-1})	rate Hofmann-product (mol s^{-1} g^{-1})	(R T)$^{-1}$ ((J mol^{-1})$^{-1}$)	ln TOF Saytzeff-product	ln TOF Hofmann-product
140	413	2.2×10^{-6}	3.5×10^{-7}	2.91×10^{-4}	-5.1	-7.0
150	423	4.6×10^{-6}	8.0×10^{-7}	2.84×10^{-4}	-4.4	-6.1
160	433	9.7×10^{-6}	2.1×10^{-6}	2.78×10^{-4}	-3.6	-5.2
170	443	2.0×10^{-5}	4.6×10^{-6}	2.72×10^{-4}	-2.9	-4.4
180	453	3.7×10^{-5}	9.5×10^{-6}	2.66×10^{-4}	-2.3	-3.6
190	463	5.9×10^{-5}	1.6×10^{-5}	2.60×10^{-4}	-1.8	-3.1

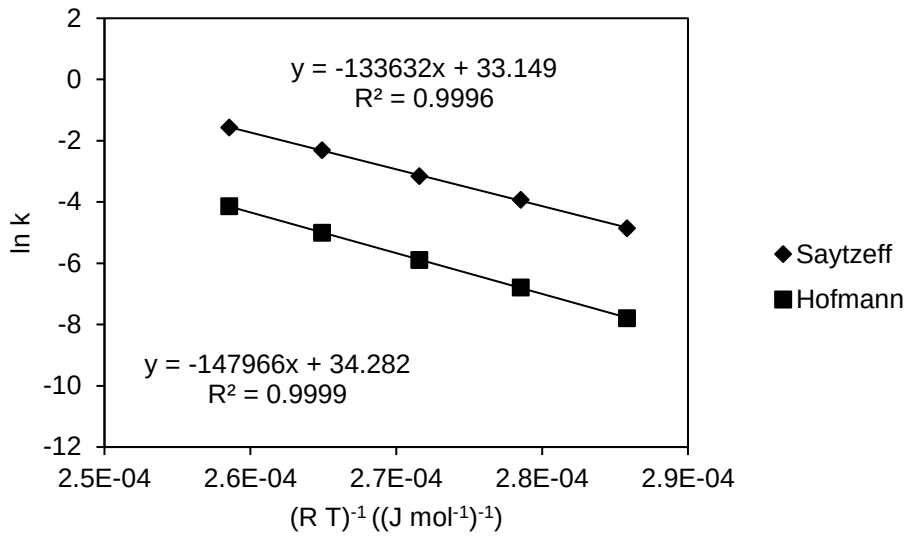

Figure S25. Arrhenius-plot: Hofmann- and Saytzeff-product (E_a = 134 and 148 kJ mol^{-1}) of **2-McyOH** (0.2 M), **H_3PO_4**.

Table S20. Dehydration rates leading to Hofmann- and Saytzeff-products of **2-McyOH** (0.5 M), **H_3PO_4**.

T (°C)	T (K)	rate Hofmann-product (mol s^{-1})	rate Saytzeff-product (mol s^{-1})	n H^+ (mol)	ln k Hofmann-product	ln k Saytzeff-product
150	423	1.5×10^{-8}	2.9×10^{-7}	1.83×10^{-4}	-7.78	-4.85
160	433	3.8×10^{-8}	6.6×10^{-7}	1.66×10^{-4}	-6.78	-3.92
170	443	8.3×10^{-8}	1.3×10^{-6}	1.51×10^{-4}	-5.89	-3.15
180	453	1.8×10^{-7}	2.7×10^{-6}	1.36×10^{-4}	-5.00	-2.31
190	463	3.9×10^{-7}	5.2×10^{-6}	1.23×10^{-4}	-4.14	-1.56

Table S21. Comparison of $\Delta H^{\circ\ddagger}$ and $\Delta S^{\circ\ddagger}$ of Saytzeff- and Hofmann-products, **MFI-45** and **H_3PO_4**.

Cat.	Substrate[a]	Saytzeff-product		Hofmann-product	
		$\Delta H^{\circ\ddagger}$ (kJ mol^{-1})	$\Delta S^{\circ\ddagger}$ (J K^{-1} mol^{-1})	$\Delta H^{\circ\ddagger}$ (kJ mol^{-1})	$\Delta S^{\circ\ddagger}$ (J K^{-1} mol^{-1})
H_3PO_4	2-McyOH	130 (±1)	+18 (±3)	144 (±1)	+28 (±1)
MFI	2-McyOH	110 (±3)	-13 (±8)	125 (±3)	+5 (±8)
MFI	2-EcyOH	100 (±3)	-33 (±6)	117 (±3)	-14 (±8)
MFI	2-PcyOH	103 (±3)	-41 (±6)	121 (±4)	-12 (±9)

[a] *Cis/trans* mixture.

Table S22. [1]H-NMR analysis of experiments with pure isomers of **2-** *and* **4-McyOH**, **MFI-45** and **H_3PO_4**.

Substrate	Catalyst	Conversion (%)	*Cis* or *trans* isomer, initial impurity (%)	*Cis* or *trans* isomer, final composition (%)	Assigned Mechanism
cis-2-McyOH	H_3PO_4	14.2	1[a]	1[a]	E2
trans-2-McyOH	H_3PO_4	29.9	3[b]	6[b]	E1
cis-4-McyOH	H_3PO_4	61.9	1[a]	41[a]	E1
trans-4-McyOH	H_3PO_4	21.1	1[b]	4[b]	E1
cis-2-McyOH	MFI	39.7	1[a]	2[a]	E2
trans-2-McyOH	MFI	64.0	0[b]	5[b]	E1
cis-4-McyOH	MFI	17.1	1[a]	8[a]	E1
trans-4-McyOH	MFI	20.1	1[b]	3[b]	E1

[a] *Trans* isomer. [b] *Cis* isomer.

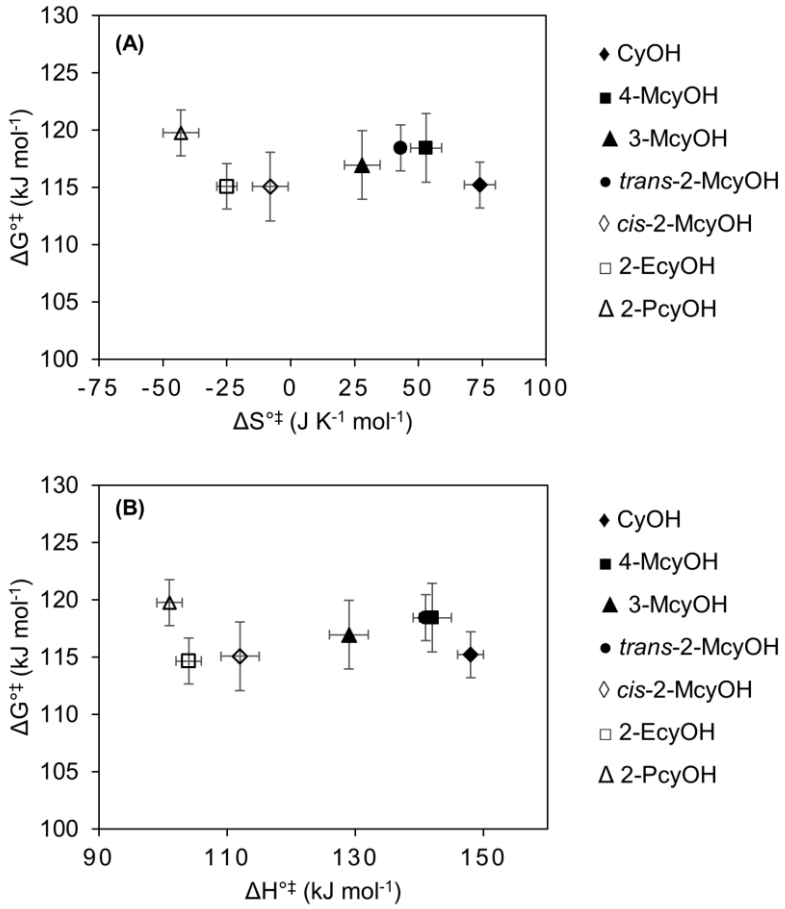

Figure S26A). Correlation of $\Delta S^{\circ\ddagger}$ and $\Delta G^{\circ\ddagger}$ for zeolite catalyzed dehydration of alkylcyclohexanols. **B**) Correlation of $\Delta H^{\circ\ddagger}$ and $\Delta G^{\circ\ddagger}$ for zeolite catalyzed dehydration of alkylcyclohexanols.

Table S23. Selectivity for the conversion of *cis/trans*-**4-McyOH** at 170 °C, MFI-45.

Conversion (%) 4-McyOH (170 °C)	Selectivity (%)			
	1-McyOH	4-Methyl-cyclohexene	1-Methyl-cyclohexene	Ethylcyclopentene
3.1	2.0	66.3	30.2	1.4
7.0	1.5	69.3	27.6	1.3
8.3	1.6	70.5	26.1	1.5
11.1	1.3	72.7	24.6	1.2

Table S24. Selectivity for the conversion of *cis/trans*-**3-McyOH** at 170 °C, MFI-45.

Conversion (%)	Selectivity (%)			
3-McyOH (170 °C)	1-McyOH	3- and 4-Methyl-cyclohexene	1-Methylcyclohexene	Ethylcyclopentene
2.4	2.0	69.2	28.1	0.6
5.7	1.7	69.0	28.9	0.4
7.9	1.5	70.4	27.9	0.3
13.4	1.4	70.3	28.0	0.3

Table S25. Selectivity for the conversion of *cis/trans*-**2-McyOH** at 170 °C, MFI-45.

Conversion (%)	Selectivity (%)			
2-McyOH (170 °C)	1-McyOH	Hofmann product	Saytzeff product	Ethylcyclopentene
5.6	5.3	13.8	80.3	0.6
10.7	5.6	13.4	80.4	0.6
13.7	4.9	13.7	80.8	0.6
18.7	4.2	14.8	80.3	0.6

Table S26. Selectivity for the conversion of *cis/trans*-**2-EcyOH** at 170 °C, MFI-45.

Conversion (%)	Selectivity (%)			
2-EcyOH (170 °C)	1-McyOH	Hofmann product	Saytzeff product	Ethylcyclopentene
5.6	4.8	8.5	85.9	0.8
12.5	3.3	8.7	87.2	0.8
17.7	2.8	9.0	87.4	0.8

Table S27. Selectivity for the conversion of *cis/trans*-**2-PcyOH** at 170 °C, MFI-45.

Conversion (%)	Selectivity (%)			
2-PcyOH (170 °C)	1-McyOH	Hofmann product	Saytzeff product	Ethylcyclopentene
3.1	1.2	16.6	80.8	1.3
6.3	1.1	17.3	80.4	1.2
9.6	1.1	17.9	79.7	1.2
13.4	1.0	18.6	79.1	1.3

Kinetics

The *conversion X* is defined as the amount of reactant, which was converted during the reaction period and is expressed as fraction of the initial amount of reactant $n_{reactant,0}$.

$$X_{reactant} = \frac{n_{reactant,0} - n_{reactant}}{n_{reactant,0}}$$

Equation S1. Conversion ($X_{reactant}$).

The *yield Y* of a product is defined as the amount of product $n_{product}$, which was formed during the reaction time from the reactant $n_{reactant,0}$.

$$Y_{product} = \frac{n_{product} - n_{product,0}}{n_{reactant,0}} \cdot \frac{|v_{reactant}|}{\sum_i v_{product}}$$

Equation S2. Yield ($Y_{product}$).

The *selectivity S* is the ratio of the yield and the conversion.

$$S_{product} = \frac{n_{product} - n_{product,0}}{\sum(n_{product} - n_{product,0})} = \frac{Y_{product}}{X_{reactant}}$$

Equation S3. Selectivity ($S_{product}$).

The *initial rates r* were determined *via* the differential method. The gradient $X \cdot t_R^{-1}$ of the graph "*conversion X (< 20%) versus reaction time* t_R" is multiplied with the initial molar amount of reactant $n_{reactant,0}$ and divided by the amount of catalyst m_{cat}.

$$r = \frac{X \cdot n_{reactant,0}}{t_R \cdot m_{cat}} \quad \left[\frac{mol}{s \cdot g}\right]$$

Equation S4. Reaction rate (r).

The *turnover frequency TOF* represents the number of converted molecules per time and per number of catalytic centers.

$$TOF = \frac{r}{c\,(H^+)} \quad \left[\frac{mol_{reactant}}{mol_{H^+} \cdot s}\right] \; or \; \left[\frac{1}{s}\right]$$

Equation S5. Turnover frequency (TOF).

The rate equation is the product of the rate constant k and the concentration of the reactant c to the power of the reaction order n.

$$r = k \cdot c^n$$

Equation S6. Rate equation.

The rate equation has to be linearized in the following way to determine the order of a chemical reaction:

$$\ln(r) = \ln(k) + n \cdot \ln(c)$$

Equation S7. Linearization of the rate equation.

The slope corresponds to the reaction order n and the intercept of the y-axis represents ln(k).

The temperature dependence of the rates are expressed by the Arrhenius equation (**Equation S8.**). The rate constant k consists of the pre-exponential factor A_{pre} and the temperature T, the universal gas constant R and the activation energy E_a in an exponential term.

$$k = A_{pre} \cdot e^{-\frac{E_a}{R \cdot T}}$$

Equation S8. The Arrhenius equation.

By linearization of the Arrhenius equation the activation energy E_a of a reaction can be determined:

$$\ln(k) = \ln\left(A_{pre}\right) - \frac{E_a}{R \cdot T}$$

Equation S9. Linearization of the Arrhenius equation.

The slope of the straight line of the ln(k) versus $(R \cdot T)^{-1}$ plot represents the activation barrier E_a and the intercept of the y-axis is $\ln(A_{pre})$.

Determination of enthalpy ($\Delta H^{\circ\ddagger}$) **and entropy** ($\Delta S^{\circ\ddagger}$) **of activation**

Equation S10. The Eyring equation, with k = TOF (rate per BAS), T = temperature (K), k_B = Boltzmann constant (1.38×10^{-23} J K^{-1}), h = Planck constant (6.63×10^{-34} J s), K = equilibrium constant.

$$k = \frac{k_B \cdot T}{h} \cdot K$$

Equation S11. Linearization of the Eyring equation.

$$k = \frac{T \cdot k_B}{h} \cdot e^{-\frac{\Delta G^{\circ\ddagger}}{R \cdot T}}$$

$$k = \frac{T \cdot k_B}{h} \cdot e^{-\frac{(\Delta H^{\circ\ddagger} - T \cdot \Delta S^{\circ\ddagger})}{R \cdot T}}$$

$$\frac{k \cdot h}{T \cdot k_B} = e^{\frac{(-\Delta H^{\circ\ddagger} + T \cdot \Delta S^{\circ\ddagger})}{R \cdot T}}$$

$$\ln\left(\frac{k \cdot h}{T \cdot k_B}\right) = \frac{-\Delta H^{\circ\ddagger} + T \cdot \Delta S^{\circ\ddagger}}{R \cdot T}$$

$$\ln\left(\frac{k \cdot h}{T \cdot k_B}\right) \cdot R = \frac{-\Delta H^{\circ\ddagger}}{T} + \Delta S^{\circ\ddagger}$$

Theoretical calculations of charge distribution in methyl substituted cyclohexyl carbenium ions

The structures of (substituted) cyclohexyl carbenium ions (cations) are fully optimized with the B3LYP functional combined with the 6–311++G (d, p) basis set as implemented in the Gaussian 09 package.[1] The partial atomic charge of each atom of the cations (**Figure S27**) are estimated using Mulliken population analysis.

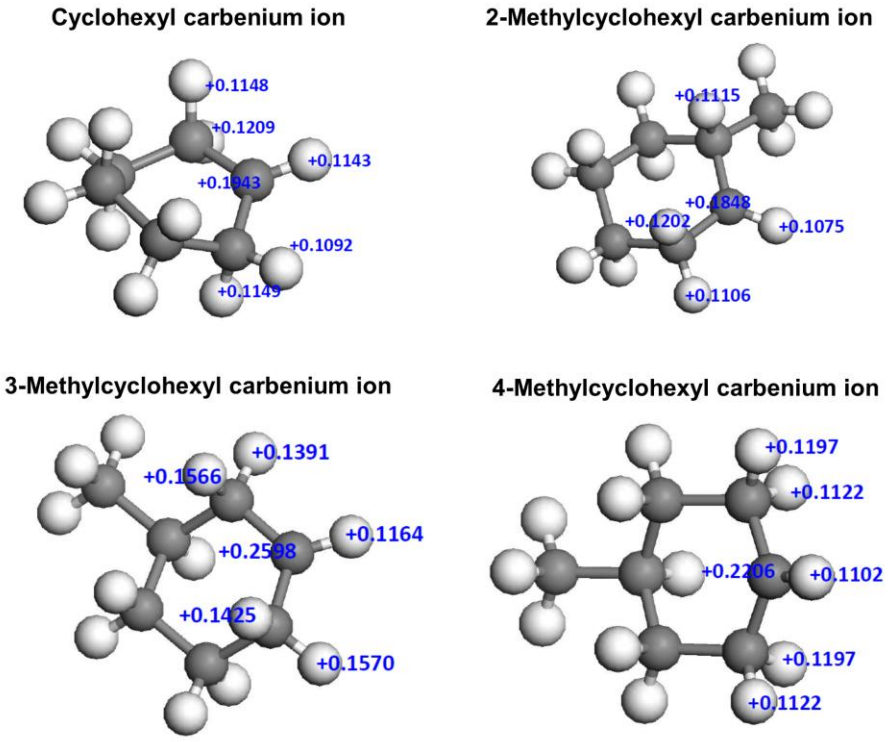

Figure S27. Partial charges of the substituted methyl cyclohexyl carbenium ions.

References

1 Frisch, M. J.; Trucks, G. W.; Schlegel, H. B.; Scuseria, G. E.; Robb, M. A.; Cheeseman, J. R.; Scalmani, G.; Barone, V.; Mennucci, B.; Petersson, G. A.; Nakatsuji, H.; Caricato, M.; Li, X.; Hratchian, H. P.; Izmaylov, A. F.; Bloino, J.; Zheng, G.; Sonnenberg, J. L.; Hada, M.; Ehara, M.; Toyota, K.; Fukuda, R.; Hasegawa, J.; Ishida, M.; Nakajima, T.; Honda, Y.; Kitao, O.; Nakai, H.; Vreven, T.; Montgomery, Jr., J. A.; Peralta, J. E.; Ogliaro, F.; Bearpark, M.; Heyd, J. J.; Brothers, E.; Kudin, K. N.; Staroverov, V. N.; Kobayashi, R.; Normand, J.; Raghavachari, K.; Rendell, A.; Burant, J. C.; Iyengar, S. S.; Tomasi, J.; Cossi, M.; Rega, N.; Millam, J. M.; Klene, M.; Knox, J. E.; Cross, J. B.; Bakken, V.; Adamo, C.; Jaramillo, J.; Gomperts, R.; Stratmann, R. E.; Yazyev, O.; Austin, A. J.; Cammi, R.; Pomelli, C.; Ochterski, J. W.; Martin, R. L.; Morokuma, K.; Zakrzewski, V. G.; Voth, G. A.; Salvador, P.; Dannenberg, J. J.; Dapprich, S.; Daniels, A. D.; Farkas, Ö.; Foresman, J. B.; Ortiz, J. V.; Cioslowski, J.; Fox, D. J. Gaussian, Inc., Wallingford CT, **2009**.